JOURNAL OF VIROLOGY, Dec. 2010, p. 12236–12244 Vol. 84, No. 23
0022-538X/10/$12.00 doi:10.1128/JVI.01579-10

Structure of a Major Antigenic Site on the Respiratory Syncytial Virus Fusion Glycoprotein in Complex with Neutralizing Antibody 101F▽†‡

Jason S. McLellan,* Man Chen, Jung-San Chang, Yongping Yang, Albert Kim, Barney S. Graham, and Peter D. Kwong

Vaccine Research Center, National Institute of Allergy and Infectious Diseases, National Institutes of Health, Bethesda, Maryland 20892

Received 28 July 2010/Accepted 20 September 2010

Respiratory syncytial virus (RSV) is a major cause of pneumonia and bronchiolitis in infants and elderly people. Currently there is no effective vaccine against RSV, but passive prophylaxis with neutralizing antibodies reduces hospitalizations. To investigate the mechanism of antibody-mediated RSV neutralization, we undertook structure-function studies of monoclonal antibody 101F, which binds a linear epitope in the RSV fusion glycoprotein. Crystal structures of the 101F antigen-binding fragment in complex with peptides from the fusion glycoprotein defined both the extent of the linear epitope and the interactions of residues that are mutated in antibody escape variants. The structure allowed for modeling of 101F in complex with trimers of the fusion glycoprotein, and the resulting models suggested that 101F may contact additional surfaces located outside the linear epitope. This hypothesis was supported by surface plasmon resonance experiments that demonstrated 101F bound the peptide epitope ~16,000-fold more weakly than the fusion glycoprotein. The modeling also showed no substantial clashes between 101F and the fusion glycoprotein in either the pre- or postfusion state, and cell-based assays indicated that 101F neutralization was not associated with blocking virus attachment. Collectively, these results provide a structural basis for RSV neutralization by antibodies that target a major antigenic site on the fusion glycoprotein.

Respiratory syncytial virus (RSV) belongs to the *Paramyxoviridae* family of enveloped, negative-sense, single-stranded RNA viruses and is a major cause of lower respiratory tract infections in infants and the elderly (14, 16). In the United States, RSV causes more than 100,000 hospitalizations annually (36), and it is estimated to cause about 160,000 deaths globally each year (2). Currently there is no vaccine for RSV, and a trial with a formalin-inactivated virus was associated with increased disease severity in infants upon infection with RSV (22). The vaccine-enhanced illness was associated with elicitation of low-avidity antibodies (11), eosinophilic infiltration (22), and immune complex deposition in small airways (35). Until a vaccine is approved, hospitalizations resulting from RSV infection can be reduced by monthly injections of the monoclonal antibody (MAb) palivizumab (Synagis) (19).

RSV-neutralizing antibodies bind to epitopes on the fusion (F) glycoprotein or the attachment (G) glycoprotein (41). Neutralizing epitopes on the F glycoprotein were originally mapped by identifying amino acids that were altered in antibody escape variants and by assessing antibody binding to RSV F-derived peptides (3). These studies demonstrated neutralizing antibodies are often targeted to two distinct linear epitopes. Antigenic site II (also called site A) includes residues 255 to 275 and is the target of palivizumab (3, 5). This epitope was predicted to be conformationally dependent (27), and the structure of a more potent derivative of palivizumab in complex with this epitope revealed that the linear epitope adopts a helix-loop-helix conformation (31). Antigenic site IV (also called site C) includes residues 422 to 438 (3, 5) and is the target of antibodies MAb19 (3) and 101F (44). MAb19 was humanized and tested in clinical trials but failed to show significant efficacy (21, 32, 38). This epitope is C-terminal to the cysteine-rich region and is part of domain II, which in homologous paramyxovirus F glycoproteins remains structurally unchanged between pre- and postfusion conformations (46).

We undertook structural and functional studies of the interaction between 101F and its epitope on the RSV F glycoprotein to investigate the mechanism of antibody-mediated RSV neutralization. Here we present the crystal structure of the antigen-binding fragment (Fab) of 101F in complex with its F glycoprotein-derived epitope peptide. The structure defined the length of the linear epitope and allowed for modeling of 101F binding to pre- and postfusion F trimers. Hypotheses based on these models were tested to investigate the mechanism of 101F neutralization and the extent of the epitope. These results are analyzed and discussed in the context of known antibody escape mutations, mechanisms of antibody-mediated virus neutralization, and applicability to epitope-specific vaccine design.

MATERIALS AND METHODS

Viruses and cells. Viral stocks were prepared and maintained as previously described (15). RSV expressing green fluorescent protein (RSV-GFP) was constructed and provided by Mark Peeples and Peter Collins, as previously reported (17). The titer of the RSV-GFP stocks used for flow cytometry-based neutral-

* Corresponding author. Mailing address: Vaccine Research Center, NIAID/NIH, 40 Convent Drive, Bldg. 40, Rm. 2613B, Bethesda, MD 20892. Phone: (301) 594-8265. Fax: (301) 480-2658. E-mail: mclellanja@mail.nih.gov.

† Supplemental material for this article may be found at http://jvi.asm.org/.

▽ Published ahead of print on 29 September 2010.

‡ The authors have paid a fee to allow immediate free access to this article.

ization and fusion assays was 2.5×10^7 PFU/ml. The titer of the RSV A2 stock used for the attachment assay was 1.02×10^8 PFU/ml.

HEp-2 cells were maintained in Eagle's minimal essential medium containing 10% fetal bovine serum (10% EMEM) and were supplemented with 2 mM glutamine, 10 U of penicillin G per ml, and 10 μg of streptomycin sulfate per ml.

Measurement of antibody-mediated neutralization. Antibody-mediated RSV neutralization was measured as described in reference 8. Briefly, RSV-GFP was added to HEp-2 cells and infection was monitored as a function of GFP expression at 18 h postinfection by flow cytometry. Data were analyzed by curve fitting and nonlinear regression (Prism; GraphPad Software Inc., San Diego, CA).

Attachment assay. The flow cytometry-based attachment assay was modified from a similar assay performed on adherent cells (6). Briefly, HEp-2 cells were dispersed into medium from plastic flasks by using a cell dissociation solution (Cellstripper; Mediatech Inc., Herndon, VA), washed with cold phosphate-buffered saline (PBS), seeded at 5×10^4/well in 96-well U-bottom plates in 10% EMEM, and chilled for 1 h at 4°C before use. Antibodies and heparin (Sigma, St. Louis, MO), a known RSV attachment inhibitor, starting from 100 μg/ml, were distributed in 11 serial 4-fold dilutions and then mixed with 5×10^6 PFU virus (RSV A2 strain) for 1 h at 37°C. Medium from chilled cells was removed after centrifugation for 5 min at 1,500 rpm, and 100-μl aliquots of virus or mixtures of virus and reagents were added to chilled cells and incubated for 1 h at 4°C. After incubation, cells were washed three times in cold PBS to remove unbound virus and then fixed with 0.5% paraformaldehyde. Viruses bound on cells were detected with a 1:1,000 dilution of fluorescein isothiocyanate-conjugated goat anti-RSV antibody (Biodesign International, Saco, ME) for 45 min at 4°C. Cells were washed in cold PBS and evaluated by flow cytometry (LSR II instrument; Becton Dickinson, San Jose, CA). Median fluorescence intensities of bound virus were analyzed with FlowJo software, version 8.5 (Tree Star, San Carlos, CA).

Virus-to-cell fusion inhibition assay. HEp-2 cells were seeded at 5×10^4/well in 96-well plates, cultured for 24 h at 37°C, and then chilled at 4°C for 1 h prior to assay. RSV-GFP was added to prechilled cells for 1 h at 4°C, and then cells were washed three times in cold PBS to remove unbound virus. Next, 100 μl of serially diluted antibodies (starting concentration, 1 mg/ml) ranging from 1:10 to 1:40,960 were added to chilled cells and incubated 1 h at 4°C before transferring to 37°C for 18 h. After incubation, cells were trypsinized to achieve a single-cell suspension, fixed in 0.5% paraformaldehyde, and analyzed on an LSR II instrument (Becton Dickinson, San Jose, CA) to determine frequencies of GFP-expressing cells. Data were analyzed with FlowJo software, version 8.5 (Tree Star, San Carlos, CA) and by curve fitting and nonlinear regression (Prism; GraphPad Software Inc., San Diego, CA) to determine the percent neutralization at a given antibody concentration and the 50% effective concentration (EC_{50}).

101F IgG cloning, expression, and purification. Two codon-optimized DNA fragments encoding the variable heavy and light chains of murine 101F (A. Del Vecchio, P. Tsui, P. J. Branigan, L. Conrad, N. Day, C. Liu, R. Sweet, S.-J. Wu, J. A. Melero, J. Luo, G. Canziani, M. Tornetta, G. Raghunathan, and V. Koka, U.S. patent application 11/261,356) were synthesized by GeneArt and cloned in-frame into pVRC8400 (4) mammalian expression vectors containing murine IgG1 heavy and light constant domains, respectively. Both vectors were cotransfected at a 1:1 ratio into HEK293F cells (Invitrogen, Carlsbad, CA) in serum-free 293Freestyle medium (Invitrogen, Carlsbad, CA). After 3 h, valproic acid (Sigma, St. Louis, MO) was added to a 4 mM final concentration. Expression lasted for 5 days at 37°C with 10% CO_2 and shaking at 125 rpm in disposable flasks. The supernatant was collected, filtered, and passed over protein G-agarose resin (Pierce, Waltham, MA). After washing with 6 column volumes of PBS, the resin was eluted with 3 column volumes of IgG elution buffer (Pierce, Waltham, MA) and immediately neutralized with 1 M Tris, pH 8.0. The eluted antibody was dialyzed against PBS and stored at 4°C.

101F Fab fragment preparation. Protein G-purified 101F IgG was reduced with 100 mM dithiothreitol at 37°C for 1 h and then alkylated with 2 mM iodoacetamide for 48 h at 4°C. Alkylated 101F IgG was digested with ficin (Sigma, St. Louis, MO) in the presence of 20 mM L-cysteine and 1 mM EDTA at 37°C for 1 h. The reaction was quenched by the addition of iodoacetamide to a final concentration of 40 mM, and then the mixture was passed over protein A-agarose. The Fab-containing flowthrough fraction was purified over a Superdex 200 gel filtration column, and concentrated aliquots were stored frozen at −80°C.

Protein crystallization and data collection. A peptide with the sequence ST ASNKNRGIIKTFS was synthesized by American Peptide with an acetylated N terminus and an amidated C terminus. This peptide corresponds to residues 422 to 436 of the RSV F glycoprotein with a C422S substitution. The peptide was dissolved in water, and a 5-fold molar excess was incubated with 101F Fab for 1.5 h at 22°C. The complex was concentrated to ~8.5 mg/ml, and 576 crystallization conditions were screened using a Cartesian Honeybee crystallization robot. Initial crystals were grown by the vapor diffusion method in sitting drops at 20°C by mixing 0.1 μl of protein complex with 0.1 μl of reservoir solution (20.5% [wt/vol] polyethylene glycol 4000 [PEG 4000], 0.2 M lithium sulfate monohydrate, 0.1 M Tris-HCl [pH 8.5]). These crystals were manually reproduced in hanging drops by mixing 0.9 μl protein complex with 0.9 μl of the initial reservoir solution containing a range of PEG 4000 concentrations. After 2 days, long rods were observed in wells containing 16% (wt/vol) PEG 4000, and these crystals were flash-frozen in liquid nitrogen in 15% (wt/vol) PEG 4000, 15% (vol/vol) 2*R*,3*R*-butanediol, 0.2 M lithium sulfate monohydrate, 0.1 M Tris-HCl (pH 8.5) and loaded into a cryopuck. Data to 1.95 Å were collected at a wavelength of 0.826 Å at the SER-CAT beamline ID-22 using the robot automounter (Advanced Photon Source; Argonne National Laboratory).

Similar procedures were used to crystallize the complex between 101F Fab and a longer peptide (STASNKNRGIIKTFSNG), corresponding to residues 422 to 438 of the RSV F glycoprotein with a C422S substitution. Data to 2.87 Å were collected at a wavelength of 1.000 Å at the SER-CAT beamline BM-22 (Advanced Photon Source; Argonne National Laboratory).

Structure determination, model building, and refinement. Diffraction data for the complex containing the shorter peptide were processed with the HKL2000 suite (33), and a molecular replacement solution consisting of two Fab molecules per asymmetric unit was obtained using PHASER (30). Model building was carried out using COOT (13), and refinement was performed with PHENIX (1). Final data collection and refinement statistics are presented in Table 1. The Ramachandran plot as determined by MOLPROBITY (10) shows 96.9% of all residues in favored regions and 99.8% of all residues in allowed regions. All structural images were created using the PyMol molecular graphics system, version 1.1 (Schrödinger, LLC).

The diffraction data for the complex containing the longer peptide were processed with the HKL2000 suite (33), and initial refinement used the coordinates of the complex containing the shorter peptide as the model (the same reflections were used in both test sets). Model building was done in COOT (13), and refinement was performed with PHENIX (1). Final data collection and refinement statistics are presented in Table 1. The Ramachandran plot as de-

TABLE 1. Data collection and refinement statistics (molecular replacement)

Parameter	101F short peptide	101F long peptide
PDB ID	3O41	3O45
Data collection		
Space group	$P2_12_12_1$	$P2_12_12_1$
Cell dimensions *a*, *b*, *c* (Å)	79.9, 93.0, 141.2	79.5, 93.0, 140.9
Resolution (Å)	50–1.95	50–2.90
R_{merge}	10.7 (47.9)[a]	25.6 (68.8)[a]
$I/\sigma I$	15.5 (2.0)[a]	7.5 (1.8)[a]
Completeness (%)	95.7 (77.4)[a]	98.7 (92.0)[a]
Redundancy	5.9 (4.3)[a]	6.9 (5.1)[a]
Refinement		
Resolution (Å)	1.95	2.87
No. of reflections	69,877	23,958
R_{work}/R_{free} (%)	17.7/21.7	20.0/25.4
No. of atoms		
Protein	6,695	6,716
Ligand/ion	225	209
Water	732	28
B-factors		
Protein	27.4	31.8
Ligand/ion	45.8	41.4
Water	35.0	11.5
RMSD		
Bond lengths (Å)	0.005	0.002
Bond angles (°)	0.941	0.558

[a] Values in parentheses are for the highest-resolution shell.

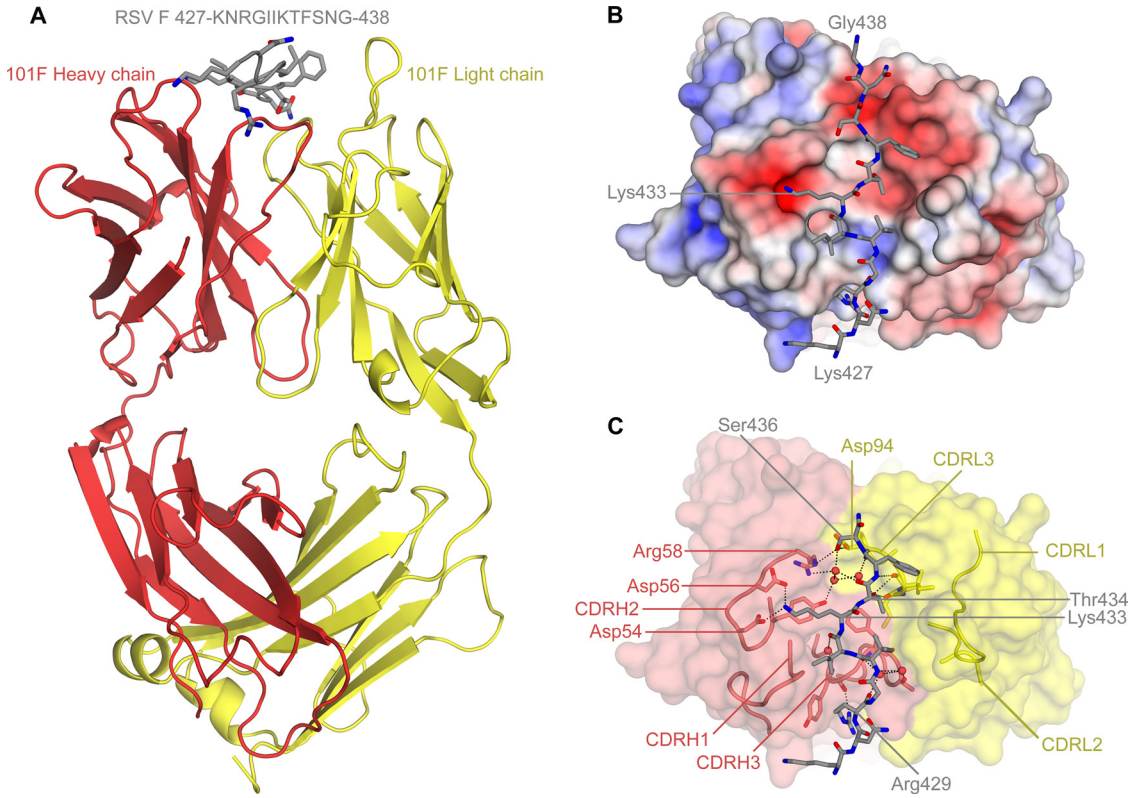

FIG. 1. Structure of 101F Fab bound to its RSV F epitope peptide. The structure defines the linear 101F epitope as RSV F residues 427 to 437 (Gly436 does not contact the Fab). The positively charged side chain of Lys433, a residue mutated in escape variants, binds to a negatively charged pocket on 101F. (A) Cα-ribbon representation of 101F Fab bound to a stick representation of the RSV F epitope peptide. The 101F heavy chain is red, the light chain is yellow, and the peptide is gray. (B) Molecular surface of 101F Fab, colored according to electrostatic potential. Potentials are colored from red to blue, −5 to +5 kT/e, respectively. The peptide is shown in stick representation, and Lys433 is labeled. The orientation is a 90° rotation of the image in panel A about the horizontal axis. (C) Interactions between the six 101F CDRs and the peptide. Shown in a transparent molecular surface of 101F Fab with ribbon representation of the six CDRs, plus Arg^{H58} from the C″ strand. The peptide is shown as sticks, as are 101F residues making hydrogen bonds or salt bridges with the peptide. Coloring is the same as for panel A. Oxygen atoms are red and nitrogen atoms are blue. Waters are shown as red spheres, and hydrogen bonds are depicted as dotted lines.

termined by MOLPROBITY (10) shows 96.3% of all residues in favored regions and 99.9% of all residues in allowed regions.

Surface plasmon resonance. All surface plasmon resonance (SPR) experiments were carried out on a Biacore 3000 instrument (GE Healthcare, Chalfont St. Giles, United Kingdom). For the detection of 101F binding to RSV F, a trimeric RSV F glycoprotein stabilized with a fibritin trimerization motif (31) was covalently coupled to a CM5 chip at 600 response units (RU), and a blank surface with no antigen was created under identical coupling conditions for use as a reference. 101F Fab was serially diluted 2-fold, starting at 25 nM, into 10 mM HEPES (pH 7.4), 150 mM NaCl, 3 mM EDTA, and 0.005% polysorbate 20 (HBS-EP) and injected over the immobilized F glycoprotein and reference cell at 50 μl/min. The surface was regenerated with 100 μl of 10 mM glycine (pH 1.5) at a flow rate of 100 μl/min. The data were processed with SCRUBBER-2 and double referenced by subtraction of the blank surface and a blank injection (no analyte). Binding curves were globally fit to a 1:1 binding model, and the equilibrium dissociation constant, K_d, was calculated by dividing the dissociation rate constant by the association rate constant.

For the detection of 101F binding to peptide, 101F IgG was covalently coupled to a CM5 chip at high density (2,150 RU), and a blank surface with no antigen was created for use as a reference. N-terminally acetylated peptide with the sequence STASNKNRGIIKTFSNGGSYGTETSQVAPA was serially diluted 2-fold, starting at 100 μM, into HBS-EP and injected over the immobilized 101F IgG and reference cell at 40 μl/min. Data were processed with SCRUBBER-2 and double referenced by subtraction of the blank surface and a blank injection. Determination of the off and on rates was not reliable due to the very fast kinetics. The equilibrium response was plotted as a function of peptide concentration and fit to a single binding-site model to determine the K_d (Prism; GraphPad Software Inc., San Diego, CA).

Protein Data Bank accession numbers. The atomic coordinates and structure factors for the 101F/peptide complexes have been deposited in the Protein Data Bank under PDB accession codes 3O41 and 3O45.

RESULTS

Structure of 101F Fab bound to its RSV F epitope peptide. Recombinant murine 101F IgG was expressed in HEK293 cells with an average yield of 8 mg/liter. RSV neutralization assays (31) demonstrated that the recombinant 101F IgG potently neutralized RSV with an EC_{50} (0.17 nM) ~3-fold lower than palivizumab (see Fig. S1 in the supplemental material). Treatment of 101F IgG with the protease ficin produced Fab fragments that could be purified to homogeneity, and these were used to facilitate crystallization.

101F Fab was incubated with a molar excess of peptide corresponding to residues 422 to 436 of the RSV F glycoprotein A2 strain (accession number P03420.1), with Cys422 replaced by Ser to prevent disulfide bond formation (STASNK NRGIIKTFS). This peptide was chosen because it was shown to give the highest 101F-binding signal in an enzyme-linked immunosorbent assay (ELISA) (44). The 101F Fab/peptide complex was screened against 576 crystallization conditions,

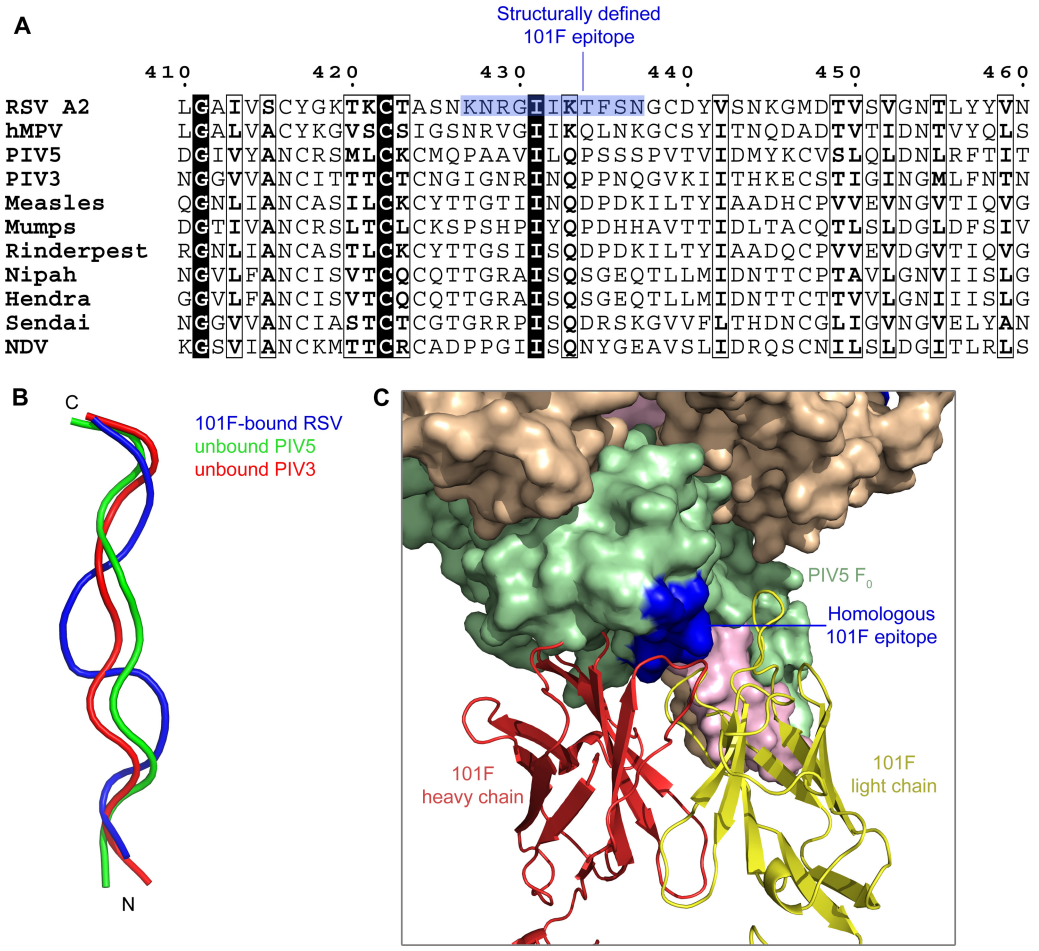

FIG. 2. Sequence and structural conservation of the 101F epitope. The 101F epitope as defined by the crystal structure exists in homologous F glycoproteins as an exposed coil. A model of 101F bound to the F glycoprotein in the prefusion conformation suggests 101F may contact residues located outside the linear epitope. (A) Multiple sequence alignment of paramyxovirus F glycoprotein fragments centered on the 101F epitope. Numbering corresponds to RSV F strain A2. Identical residues are in white text with black boxes, and conserved residues are in bold black text with outlined boxes. RSV F residues bound to 101F in the crystal structure are highlighted in blue. (B) Cα superposition of 101F-bound RSV F residues 428 to 436 and the corresponding residues from the parainfluenza virus 5 (PIV5) and PIV3 F crystal structures. (C) Model of 101F Fab bound to PIV5, based on the superposition in panel B. Residues in CDRH1, CDRH2, and CDRL1 may contact the F protein outside the linear epitope.

and crystals formed under multiple conditions. After optimization, crystals of the complex in space group $P2_12_12_1$ diffracted X-rays to 1.95 Å. A molecular replacement solution was obtained containing two Fab molecules per asymmetric unit by using fragments from three Fab structures as search models (20, 34, 42). Initial maps showed continuous electron density near the Fab combining region that we modeled as peptide. The high resolution of the data allowed for unambiguous placement of the peptide (see Fig. S2 in the supplemental material), and the structure was refined to an R_{crys}/R_{free} ratio of 17.7%/21.7%. Data collection and refinement statistics are presented in Table 1.

The N-terminal five amino acids of the peptide were disordered in the structure, and weak electron density was observed for Lys427. The C terminus of the peptide, Ser436, was very well ordered and bound near the middle of the 101F combining region (see Fig. S2 in the supplemental material), suggesting that the complete 101F epitope may extend several residues beyond Ser436. To investigate this, we crystallized 101F Fab in complex with a longer peptide that included RSV F residues Asn437 and Gly438. These crystals diffracted X-rays to 2.87 Å, and the structure was refined to an R_{crys}/R_{free} ratio of 20.0%/25.4% (Table 1; Fig. 1A). Asn437 was well ordered in both molecules in the asymmetric unit, but Gly438 was only ordered in one and it made no contacts with 101F. Thus, based on the structure, the linear 101F epitope spans RSV F residues 427 to 437 (KNRGIIKTFSN). This is similar to the minimal 101F epitope defined by peptide mapping, which consisted of residues 423 to 436 (44). In our structure, however, we did not observe electron density for residues N-terminal to Lys 427. Therefore, if these residues do bind 101F, it's likely that these interactions are weak.

Interactions between 101F and the epitope peptide. To understand the structural basis for the binding of 101F to the RSV F glycoprotein, we analyzed the interactions between 101F and the peptide. The structure with the longer peptide

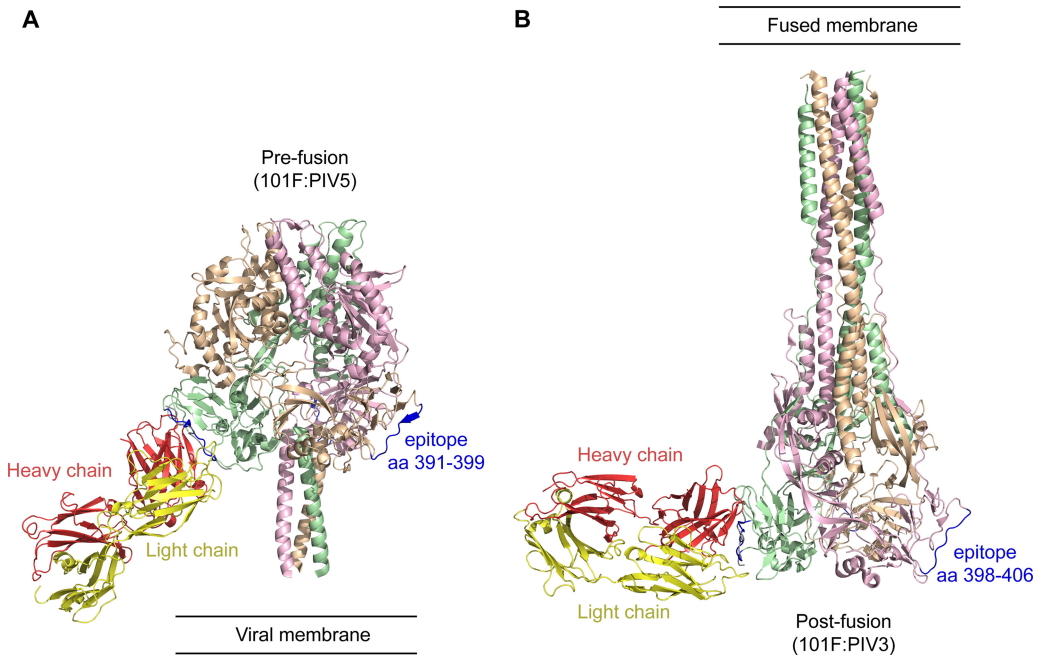

FIG. 3. Models of 101F bound to trimeric F glycoproteins. 101F is predicted to bind with similar affinity to both the pre- and postfusion conformations. (A) Model of 101F Fab bound to parainfluenza virus 5 (PIV5) in the prefusion conformation based on superposition of peptide residues 428 to 436 and PIV5 residues 391 to 399 (blue). (B) Model of 101F Fab bound to PIV3 in the postfusion conformation, based on superposition of peptide residues 428 to 436 with PIV3 residues 398 to 406 (blue). Domain II, containing the homologous 101F epitope, is in an orientation similar to that shown in panel A.

will be described unless noted otherwise. The peptide spans the length of the interface between the heavy and light chains, lying in a groove with sides formed by CDRL1 on one side and CDRH1 and CDRH2 on the other and a floor made up of the CDR3s from the heavy and light chains (Fig. 1A). The Fab-peptide interface buries 1,361 Å^2 of surface area, with 734 Å^2 buried on the peptide, 395 Å^2 on the heavy chain, and 232 Å^2 on the light chain (as calculated by using PISA [23]), values consistent with antibody-antigen interfaces (26). The Fab-peptide interface also displays a high degree of shape complementarity, as indicated by its shape correlation (S_c) value of 0.70, which is higher than the standard range of 0.64 to 0.68 for antibody/antigen complexes (24). The electrostatic potential complementarity, however, is weak, although a negatively charged pocket on CDRH2 formed by Asp^{H54} and Asp^{H56} binds the positively charged side chain of peptide residue Lys433 (Fig. 1B).

The high-resolution structure containing the shorter peptide allows for a detailed description of the interactions between 101F and the peptide, including the positions of six interface water molecules (Fig. 1C). Starting at the N terminus of the peptide, the first ordered residue is Lys427 which, along with Asn428, makes only minimal contact with the 101F heavy chain. The side chain of Arg429, however, extends down toward 101F and makes a hydrogen bond with the carbonyl oxygen of Tyr^{H96}. Gly430 makes minimal contact with 101F, but Ile431 and Ile432 make hydrophobic contacts and the carbonyl oxygen of Ile431 makes a hydrogen bond to the amide nitrogen of Phe^{H98}. The side chain of Lys433 forms a salt bridge with the side chains of both Asp^{H54} and Asp^{H56}, and the side chain of Thr434 makes hydrogen bonds to the carbonyl oxygens of Ile^{L91} and Ile^{L92}. Although the side chain of Phe435 points away from 101F, its amide nitrogen and carbonyl oxygen form hydrogen bonds with the carbonyl oxygen and amide nitrogen of Ile^{L92} and Asp^{L94}, respectively. The hydroxyl group of Ser436 makes hydrogen bonds to the side chains of Arg^{H58} and Asp^{L94}, which are part of an intricate network of hydrogen bonds involving three water molecules. In the complex with the longer peptide, Asn437 has approximately one-third of its accessible surface area buried by the 101F light chain but does not form any hydrogen bonds to the Fab.

The specific interactions observed in the crystal structure agree well with published biochemical data. Peptides containing a K433E, K433T, or R429E mutation were shown to ablate 101F binding (44). In our structure, Lys433 makes a salt bridge with the side chains of both Asp^{H54} and Asp^{H56} (see Fig. 3 below), and mutation to Glu or Thr would eliminate this interaction. Also in our structure, the side chain of Arg429 makes a hydrogen bond with the carbonyl oxygen of Tyr^{H96} and intercalates between the side chains of Tyr^{H96} and Tyr^{H100}. Although the R429E mutation could still preserve the hydrogen bond to Tyr^{H96}, the intercalation would be lost. In contrast, a peptide containing a K427E mutation had only a modest reduction in 101F binding (44), consistent with our structure, which shows that the side chain of Lys427 makes no specific interactions with 101F.

The binding of 101F to mutant RSV F glycoproteins expressed on the cell surface has also been measured (25). The largest decrease in 101F binding was observed for F glycoproteins containing mutations to Lys433. Modest reductions in binding were observed for conservative mutations to Ile431 (Ala, Leu) and Ile432 (Leu, Gln), consistent with our structure,

which shows that the side chains of Ile431 and Ile432 do not make specific interactions with 101F but rather make hydrophobic contacts. No decrease in 101F binding was observed to F glycoproteins containing the mutation N428D or N428Q (25), and this agrees well with the structure, which shows Asn428 makes only minimal contact with 101F. Thus, the structure of 101F in complex with its peptide epitope is consistent with cell-based F glycoprotein-binding data, suggesting that the peptide conformation observed in the crystal structure is similar to its conformation in the context of the F glycoprotein when bound by 101F.

Models of 101F bound to F glycoproteins. Although the structure of the RSV F glycoprotein has not yet been determined, crystal structures have been determined for related paramyxovirus F glycoproteins in both pre- and postfusion conformations (7, 37, 45, 46). We sought to create models of 101F bound to these structures in order to identify possible mechanisms of neutralization. A multiple sequence alignment of paramyxovirus F glycoproteins was created to identify the residues corresponding to the 101F epitope and to assess the degree of conservation (Fig. 2A). We found a low degree of sequence homology in the region of the F glycoprotein corresponding to the 101F epitope, with the exception of Ile431, which is strictly conserved in F glycoproteins. Inspection of the available F glycoprotein structures revealed that this residue packs against the residue corresponding to Val442, which is also highly conserved (Val, Ile, or Leu) and lies just outside the 101F epitope.

Despite the low degree of sequence conservation, the 101F epitope as defined by the crystal structure maps onto an exposed loop in both pre- and postfusion structures (Fig. 2B). Superposition of residues homologous to RSV F residues 428 to 436 showed that PIV5 and PIV3 are more similar to each other (root mean square deviation [RMSD], 1.10 Å for nine Cα atoms) than they are to the 101F-bound peptide (RMSD for PIV5, 2.14 Å; RMSD for PIV3, 1.98 Å). This may reflect the higher degree of sequence conservation between PIV5 and PIV3, as well as conformational changes in RSV F resulting from 101F binding. Models of 101F bound to the F glycoproteins were generated by orienting the Fab via superposition of the bound peptide onto the corresponding epitope in the prefusion PIV5 and postfusion PIV3 F glycoprotein structures (Fig. 3). The resulting models showed no major clashes between 101F and the F glycoproteins in either conformation, suggesting 101F binds the two conformations with similar affinity. In addition, the CDRH1, CDRH2, and CDRL1 loops are in close proximity to, or clash with, F glycoprotein residues located outside the linear epitope (Fig. 2C). This suggests that the 101F epitope may be more complex than the previously defined linear region.

101F-binding affinity. To determine whether additional residues outside the linear epitope are part of the 101F-binding site, the affinities of 101F for the F glycoprotein and peptide were determined. SPR was used to measure the binding of 101F Fab to an immobilized F glycoprotein trimer (31), and the K_d was determined to be 3.6 nM (Fig. 4A). Similarly, SPR was used to measure the binding of a peptide containing RSV F residues 422 to 438 to immobilized 101F IgG, and the K_d was determined to be 58.4 μM (Fig. 4B). This approximately 16,000-fold difference in affinity supports the hypothesis that additional residues on the RSV F glycoprotein bind 101F and are required for the high-affinity interaction. Some fraction of this decrease, however, may also be due to the loss of conformational entropy that occurs when the flexible peptide adopts a single conformation upon binding 101F. Interestingly, a similar result has been observed for motavizumab, the more potent derivative of palivizumab, which binds the RSV F glycoprotein with a K_d of 35 pM (43) but only binds its epitope peptide with a K_d of 230 nM (G. I. Tous, M. A. Schenerman, J. Casas-Finet, Z. Wei, and D. S. Pfarr, U.S. patent application 11/230,593).

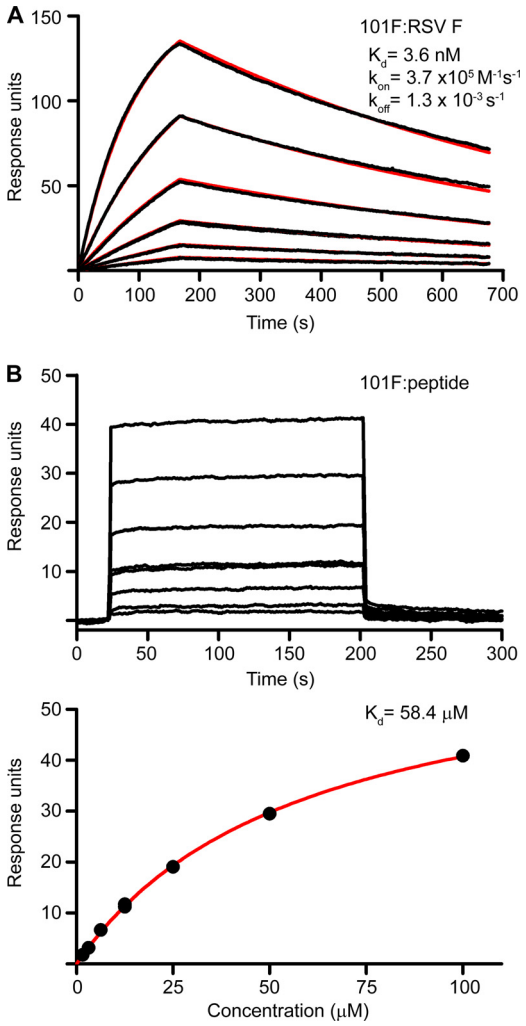

FIG. 4. 101F binding to RSV F glycoprotein and epitope peptide. 101F binds the RSV F glycoprotein 16,000-fold tighter than the epitope peptide, suggesting the 101F epitope is more complex than the linear region. (A) SPR sensorgram of 101F Fab binding to immobilized RSV F. Five 2-fold dilutions of 101F Fab starting at 25 nM were measured, plus a 3.125 nM duplicate. Red lines represent best fits of kinetic data to a 1:1 Langmuir binding model. (B, top) SPR sensorgram of peptide binding to immobilized 101F IgG. Six 2-fold dilutions of peptide starting at 100 μM were measured, plus a 12.5 μM duplicate. Binding kinetics were too fast to accurately determine rate constants. (Bottom) Plot of equilibrium response as a function of peptide concentration. The red line represents the best fit of the data to the single-site equilibrium binding model.

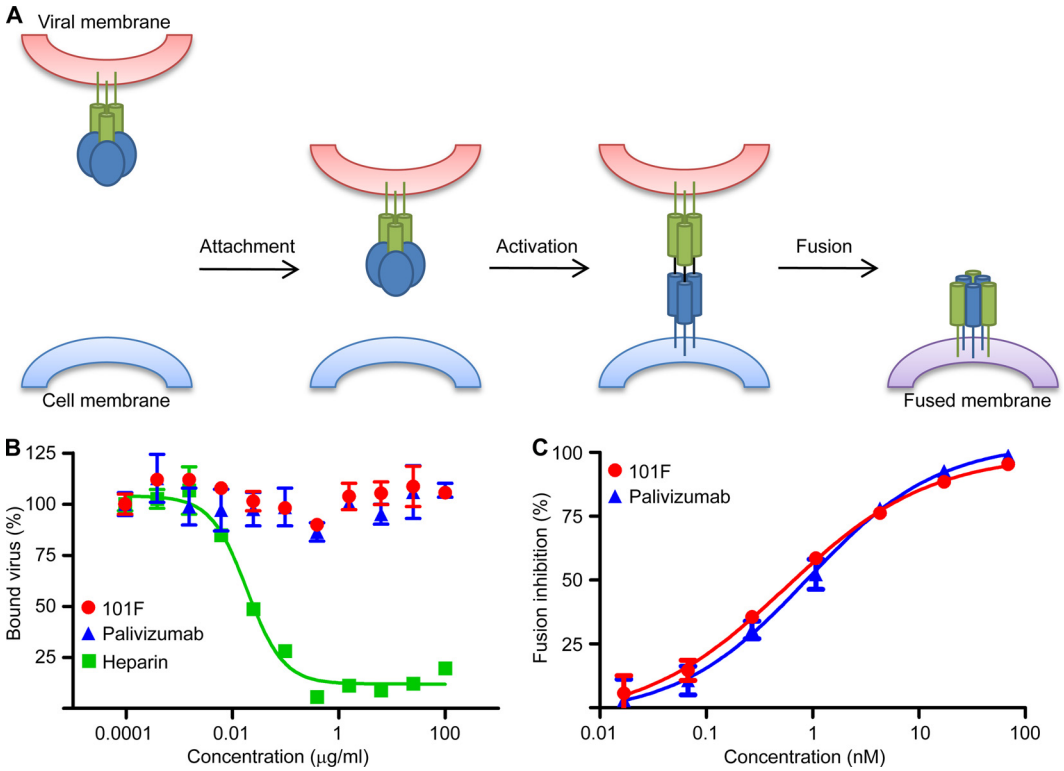

FIG. 5. 101F attachment and fusion inhibition assays. 101F prevents membrane fusion by blocking a step after viral attachment. (A) Schematic depicting virus entry into a cell. After virus attachment, the fusion glycoprotein is triggered and begins folding into the postfusion conformation, driving the fusion of the virus and cell membranes (B) 101F was added to virions prior to incubation with HEp-2 cells. The relative amount of virus bound to HEp-2 cells is plotted as a function of 101F concentration. Heparin served as a positive control and palivizumab as a negative control. (C) Antibody was added after virus attachment to HEp-2 cells. Relative amount of virus fusion inhibition (neutralization) is plotted as a function of antibody concentration. Palivizumab served as a positive control. For both panels, experiments were performed in duplicate, and plotted data represent means ± standard errors of the means.

Temporal characterization of 101F neutralization. Based on our modeling, 101F binding appears compatible with both the pre- and postfusion conformations of the F glycoprotein, suggesting 101F may neutralize RSV by some mechanism other than preventing conformational changes in the F glycoprotein. Virus neutralization can be achieved by blocking virus entry at any of the steps between attachment and membrane fusion (Fig. 5A). The receptor for RSV has yet to be identified, and even though the G glycoprotein is associated with attachment to glycosaminoglycans or C-type lectins, it is dispensable for RSV replication *in vitro*, though it appears to be important for replication *in vivo* (39). To determine whether 101F blocks virus attachment to cells, RSV virions were incubated with increasing amounts of 101F prior to incubation with HEp-2 cells at 4°C. After washing away unbound virus, the amount of bound virus was measured by flow cytometry using an anti-RSV polyclonal antibody for detection. 101F had a negligible effect on virus attachment even at a concentration of 100 μg/ml (Fig. 5B). This was similar to the effect produced by palivizumab, which has been shown to inhibit fusion and not virus attachment (18). In contrast, heparin is known to block the attachment of RSV to cells (17), and it decreased the amount of bound virus by 80%, with an EC_{50} of 0.019 μg/ml. These data suggest that 101F does not neutralize RSV via attachment inhibition.

To determine whether 101F neutralizes RSV after virus attachment to cells, GFP-expressing RSV particles were incubated with HEp-2 cells at 4°C, a temperature that allows virus attachment but prevents membrane fusion. 101F was then added, and after incubation at the fusion-permissive temperature of 37°C, the amount of GFP expressed from the viral genome was quantified by flow cytometry. The addition of 101F decreased membrane fusion to background levels, with an EC_{50} of 3.6 nM, which was similar to the palivizumab control (EC_{50}, 7.8 nM) (Fig. 5C). These data indicate that the 101F epitope is present after the virus attaches to cells and that 101F neutralizes RSV by blocking one of the steps after virus attachment.

DISCUSSION

Passive prophylaxis with neutralizing antibodies such as palivizumab is currently the best method for preventing severe disease caused by RSV. We hypothesize that structural characterization of the epitopes on the RSV F glycoprotein targeted by these antibodies will help elucidate their mechanism of action and facilitate the design of more potent antibodies and epitope-specific vaccines.

The 101F epitope on the RSV F glycoprotein is a common target of neutralizing antibodies (3, 5, 28). Antibodies targeted

to this site have produced several antibody escape mutations in the F glycoprotein, such as R429S, I432T, K433T, and S436F (3, 28). All four of these residues are observed in our crystal structure of 101F Fab bound to its epitope peptide, and each makes contact with 101F. Thus, although the complete epitope likely includes residues located outside the linear region, the location of the escape mutations suggests that the peptide represents a majority of the epitope. Additionally, as these known escape mutations for other RSV neutralizing antibodies are predicted to disrupt 101F binding, a common binding mode is suggested for antibodies targeted to this antigenic site.

After paramyxoviruses attach to the cell, triggering of the prefusion state leads to formation of a prehairpin intermediate, wherein the fusion peptides are inserted into the target cell membrane. The target cell membrane and viral membrane are pulled into close proximity as the prehairpin intermediate collapses into the hairpin intermediate and the six-helix bundle begins to form. The membranes then fuse as the fusion glycoprotein adopts the postfusion conformation. During the entry process, there are several steps which neutralizing antibodies can block, including attachment, triggering, and transition of the fusion glycoprotein to the postfusion state. We have demonstrated that 101F does not block virus attachment over a wide range of concentrations (Fig. 5B), which agrees with recently published data showing a similar result at a single antibody concentration (29). We have also shown that 101F is capable of preventing infection once the virus has attached to the cell (Fig. 5C). This narrows the window of 101F neutralization to some point between triggering of the fusion glycoprotein and transition to the postfusion state. In addition, since our modeling studies show that 101F binding is compatible with both the pre- and postfusion states (Fig. 3), 101F is predicted to bind all forms of the fusion glycoprotein, including intermediates. Thus, we propose that 101F also does not prevent triggering but rather prevents adoption of the postfusion conformation due to its bulk in the context of the cell and viral membranes.

Classical approaches to creating an RSV vaccine have been unsuccessful thus far (40), and alternative approaches are needed. One proposed method for creating vaccines against viruses that have resisted classical methods, such as HIV-1, is to use structural information of neutralizing epitopes to create immunogens that elicit antibodies targeted solely to those epitopes (12). The structural information allows the epitope to be presented to the immune system in a conformation that enables binding, and thus elicitation, of neutralizing antibodies. This has been tried with some success with anti-HIV antibodies 2F5 and 4E10 (9), which target linear epitopes in the membrane-proximal region of gp41. Although this approach may work for the 101F epitope when using the structural data presented here, our modeling and binding data suggest that residues located outside the linear epitope are required for high-affinity 101F binding. Thus, elicitation of 101F-like antibodies will likely require immunogens that consist of more than the linear portion of the epitope.

ACKNOWLEDGMENTS

We thank members of the Structural Biology Section and Structural Bioinformatics Core at the Vaccine Research Center for helpful comments and the staff at Southeast Regional Collaborative Access Team (SER-CAT) for help with X-ray diffraction data collection.

Support for this work was provided by the Intramural Research Program (National Institute of Allergy and Infectious Diseases). Use of sector 22 (SER-CAT) at the Advanced Photon Source was supported by the U.S. Department of Energy, Basic Energy Sciences, Office of Science, under contract W-31-109-Eng-38.

J.S.M. prepared, crystallized, and solved the structure of the 101F Fab/peptide complexes and performed the SPR experiments. M.C. and J.-S.C. performed the neutralization, attachment, and fusion inhibition experiments. Y.Y. and A.K. performed the expression of 101F IgG. J.S.M., M.C., B.S.G., and P.D.K. designed experiments and analyzed data. J.S.M. wrote the initial draft of the paper, on which all authors commented.

REFERENCES

1. **Adams, P. D., R. W. Grosse-Kunstleve, L.-W. Hung, T. R. Ioerger, A. J. McCoy, N. W. Moriarty, R. J. Read, J. C. Sacchettini, N. K. Sauter, and T. C. Terwilliger.** 2002. PHENIX: building new software for automated crystallographic structure determination. Acta Crystallogr. D Biol. Crystallogr. **58:** 1948–1954.
2. **Anonymous.** 2009. Initiative for vaccine research. Respiratory syncytial virus and parainfluenza viruses. World Health Organization, Geneva, Switzerland. http://www.who.int/vaccine_research/diseases/ari/en/index2.html.
3. **Arbiza, J., G. Taylor, J. A. Lopez, J. Furze, S. Wyld, P. Whyte, E. J. Stott, G. Wertz, W. Sullender, M. Trudel, and J. A. Melero.** 1992. Characterization of two antigenic sites recognized by neutralizing monoclonal antibodies directed against the fusion glycoprotein of human respiratory syncytial virus. J. Gen. Virol. **73:**2225–2234.
4. **Barouch, D. H., Z.-Y. Yang, W.-P. Kong, B. Korioth-Schmitz, S. M. Sumida, D. M. Truitt, M. G. Kishko, J. C. Arthur, A. Miura, J. R. Mascola, N. L. Letvin, and G. J. Nabel.** 2005. A human T-cell leukemia virus type 1 regulatory element enhances the immunogenicity of human immunodeficiency virus type 1 DNA vaccines in mice and nonhuman primates. J. Virol. **79:** 8828–8834.
5. **Beeler, J. A., and K. van Wyke Coelingh.** 1989. Neutralization epitopes of the F glycoprotein of respiratory syncytial virus: effect of mutation upon fusion function. J. Virol. **63:**2941–2950.
6. **Budge, P. J., Y. Li, J. A. Beeler, and B. S. Graham.** 2004. RhoA-derived peptide dimers share mechanistic properties with other polyanionic inhibitors of respiratory syncytial virus (RSV), including disruption of viral attachment and dependence on RSV G. J. Virol. **78:**5015–5022.
7. **Chen, L., J. J. Gorman, J. McKimm-Breschkin, L. J. Lawrence, P. A. Tulloch, B. J. Smith, P. M. Colman, and M. C. Lawrence.** 2001. The structure of the fusion glycoprotein of Newcastle disease virus suggests a novel paradigm for the molecular mechanism of membrane fusion. Structure **9:**255–266.
8. **Chen, M., J. S. Chang, M. Nason, D. Rangel, J. G. Gall, B. S. Graham, and J. E. Ledgerwood.** 19 August 2010. A flow cytometry-based assay to assess RSV-specific neutralizing antibody is reproducible, efficient and accurate. J. Immunol. Methods. doi:10.1016/j.jim.2010.08.005.
9. **Correia, B. E., Y.-E. A. Ban, M. A. Holmes, H. Xu, K. Ellingson, Z. Kraft, C. Carrico, E. Boni, D. N. Sather, C. Zenobia, K. Y. Burke, T. Bradley-Hewitt, J. F. Bruhn-Johannsen, O. Kalyuzhniy, D. Baker, R. K. Strong, L. Stamatatos, and W. R. Schief.** 2010. Computational design of epitope-scaffolds allows induction of antibodies specific for a poorly immunogenic HIV vaccine epitope. Structure **18:**1116–1126.
10. **Davis, I. W., A. Leaver-Fay, V. B. Chen, J. N. Block, G. J. Kapral, X. Wang, L. W. Murray, W. B. Arendall III, J. Snoeyink, J. S. Richardson, and D. C. Richardson.** 2007. MolProbity: all-atom contacts and structure validation for proteins and nucleic acids. Nucleic Acids Res. **35:**W375–W383.
11. **Delgado, M. F., S. Coviello, A. C. Monsalvo, G. A. Melendi, J. Z. Hernandez, J. P. Batalle, L. Diaz, A. Trento, H.-Y. Chang, W. Mitzner, J. Ravetch, J. A. Melero, P. M. Irusta, and F. P. Polack.** 2009. Lack of antibody affinity maturation due to poor Toll-like receptor stimulation leads to enhanced respiratory syncytial virus disease. Nat. Med. **15:**34–41.
12. **Dormitzer, P. R., J. B. Ulmer, and R. Rappuoli.** 2008. Structure-based antigen design: a strategy for next generation vaccines. Trends Biotechnol. **26:**659–667.
13. **Emsley, P., and K. Cowtan.** 2004. COOT: model-building tools for molecular graphics. Acta Crystallogr. D Biol. Crystallogr. **60:**2126–2132.
14. **Falsey, A. R., and E. E. Walsh.** 2005. Respiratory syncytial virus infection in elderly adults. Drugs Aging **22:**577–587.
15. **Graham, B. S., M. D. Perkins, P. F. Wright, and D. T. Karzon.** 1988. Primary respiratory syncytial virus infection in mice. J. Med. Virol. **26:**153–162.
16. **Hall, C. B., G. A. Weinberg, M. K. Iwane, A. K. Blumkin, K. M. Edwards, M. A. Staat, P. Auinger, M. R. Griffin, K. A. Poehling, D. Erdman, C. G. Grijalva, Y. Zhu, and P. Szilagyi.** 2009. The burden of respiratory syncytial virus infection in young children. N. Engl. J. Med. **360:**588–598.
17. **Hallak, L. K., P. L. Collins, W. Knudson, and M. E. Peeples.** 2000. Iduronic

acid-containing glycosaminoglycans on target cells are required for efficient respiratory syncytial virus infection. Virology **271:**264–275.
18. **Huang, K., L. Incognito, X. Cheng, N. D. Ulbrandt, and H. Wu.** 2010. Respiratory syncytial virus-neutralizing monoclonal antibodies motavizumab and palivizumab inhibit fusion. J. Virol. **84:**8132–8140.
19. **IMpact-RSV Study Group.** 1998. Palivizumab, a humanized respiratory syncytial virus monoclonal antibody, reduces hospitalization from respiratory syncytial virus infection in high-risk infants. Pediatrics **102:**531–537.
20. **Ito, S., T. Takayama, H. Hanzawa, K. Ichikawa, J. Ohsumi, N. Serizawa, T. Hata, and H. Haruyama.** 2002. Crystal structure of the antigen-binding fragment of apoptosis-inducing mouse anti-human Fas monoclonal antibody HFE7A. J. Biochem. **131:**137–143.
21. **Johnson, S., S. D. Griego, D. S. Pfarr, M. L. Doyle, R. Woods, D. Carlin, G. A. Prince, S. Koenig, J. F. Young, and S. B. Dillon.** 1999. A direct comparison of the activities of two humanized respiratory syncytial virus monoclonal antibodies: MEDI-493 and RSHZI9. J. Infect. Dis. **180:**35–40.
22. **Kim, H. W., J. G. Canchola, C. D. Brandt, G. Pyles, R. M. Chanock, K. Jensen, and R. H. Parrott.** 1969. Respiratory syncytial virus disease in infants despite prior administration of antigenic inactivated vaccine. Am. J. Epidemiol. **89:**422–434.
23. **Krissinel, E., and K. Henrick.** 2007. Inference of macromolecular assemblies from crystalline state. J. Mol. Biol. **372:**774–797.
24. **Lawrence, M. C., and P. M. Colman.** 1993. Shape complementarity at protein/protein interfaces. J. Mol. Biol. **234:**946–950.
25. **Liu, C., N. Day, P. Branigan, L. Gutshall, R. Sarisky, and A. Del Vecchio.** 2007. Relationship between the loss of neutralizing antibody binding and fusion activity of the F protein of human respiratory syncytial virus. Virol. J. **4:**71.
26. **Lo Conte, L., C. Chothia, and J. Janin.** 1999. The atomic structure of protein-protein recognition sites. J. Mol. Biol. **285:**2177–2198.
27. **Lopez, J. A., D. Andreu, C. Carreno, P. Whyte, G. Taylor, and J. A. Melero.** 1993. Conformational constraints of conserved neutralizing epitopes from a major antigenic area of human respiratory syncytial virus fusion glycoprotein. J. Gen. Virol. **74:**2567–2577.
28. **Lopez, J. A., R. Bustos, C. Orvell, M. Berois, J. Arbiza, B. Garcia-Barreno, and J. A. Melero.** 1998. Antigenic structure of human respiratory syncytial virus fusion glycoprotein. J. Virol. **72:**6922–6928.
29. **Magro, M., D. Andreu, P. Gomez-Puertas, J. A. Melero, and C. Palomo.** 2010. Neutralization of human respiratory syncytial virus infectivity by antibodies and low-molecular-weight compounds targeted against the fusion glycoprotein. J. Virol. **84:**7970–7982.
30. **McCoy, A. J., R. W. Grosse-Kunstleve, P. D. Adams, M. D. Winn, L. C. Storoni, and R. J. Read.** 2007. Phaser crystallographic software. J. Appl. Crystallogr. **40:**658–674.
31. **McLellan, J. S., M. Chen, A. Kim, Y. Yang, B. S. Graham, and P. D. Kwong.** 2010. Structural basis of respiratory syncytial virus neutralization by motavizumab. Nat. Struct. Mol. Biol. **17:**248–250.
32. **Meissner, H. C., J. R. Groothuis, W. J. Rodriguez, R. C. Welliver, G. Hogg, P. H. Gray, R. Loh, E. A. F. Simoes, P. Sly, A. K. Miller, A. I. Nichols, D. K. Jorkasky, D. E. Everitt, and K. A. Thompson.** 1999. Safety and pharmacokinetics of an intramuscular monoclonal antibody (SB 209763) against respiratory syncytial virus (RSV) in infants and young children at risk for severe RSV disease. Antimicrob. Agents Chemother. **43:**1183–1188.
33. **Otwinowski, Z., and W. Minor.** 1997. Processing of X-ray diffraction data collected in oscillation mode. Methods Enzymol. **276:**307–326.
34. **Padavattan, S., T. Schirmer, M. Schmidt, C. Akdis, R. Valenta, I. Mittermann, L. Soldatova, J. Slater, U. Mueller, and Z. Markovic-Housley.** 2007. Identification of a B-cell epitope of hyaluronidase, a major bee venom allergen, from its crystal structure in complex with a specific Fab. J. Mol. Biol. **368:**742–752.
35. **Polack, F. P., M. N. Teng, P. L. Collins, G. A. Prince, M. Exner, H. Regele, D. D. Lirman, R. Rabold, S. J. Hoffman, C. L. Karp, S. R. Kleeberger, M. Wills-Karp, and R. A. Karron.** 2002. A role for immune complexes in enhanced respiratory syncytial virus disease. J. Exp. Med. **196:**859–865.
36. **Shay, D. K., R. C. Holman, R. D. Newman, L. L. Liu, J. W. Stout, and L. J. Anderson.** 1999. Bronchiolitis-associated hospitalizations among US children, 1980–1996. JAMA **282:**1440–1446.
37. **Swanson, K., X. Wen, G. P. Leser, R. G. Paterson, R. A. Lamb, and T. S. Jardetzky.** 2010. Structure of the Newcastle disease virus F protein in the post-fusion conformation. Virology **402:**372–379.
38. **Tempest, P. R., P. Bremner, M. Lambert, G. Taylor, J. M. Furze, F. J. Carr, and W. J. Harris.** 1991. Reshaping a human monoclonal antibody to inhibit human respiratory syncytial virus infection in vivo. Biotechnology **9:**266–271.
39. **Teng, M. N., S. S. Whitehead, and P. L. Collins.** 2001. Contribution of the respiratory syncytial virus G glycoprotein and its secreted and membrane-bound forms to virus replication in vitro and in vivo. Virology **289:**283–296.
40. **van Drunen Littlel-van den Hurk, S., J. W. Mapletoft, N. Arsic, and J. Kovacs-Nolan.** 2007. Immunopathology of RSV infection: prospects for developing vaccines without this complication. Rev. Med. Virol. **17:**5–34.
41. **Walsh, E. E., and J. Hruska.** 1983. Monoclonal antibodies to respiratory syncytial virus proteins: identification of the fusion protein. J. Virol. **47:**171–177.
42. **Wright, L. M., A. M. Brzozowski, R. E. Hubbard, A. C. Pike, S. M. Roberts, R. N. Skovgaard, I. Svendsen, H. Vissing, and R. P. Bywater.** 2000. Structure of Fab hGR-2 F6, a competitive antagonist of the glucagon receptor. Acta Crystallogr. D Biol. Crystallogr. **56:**573–580.
43. **Wu, H., D. S. Pfarr, S. Johnson, Y. A. Brewah, R. M. Woods, N. K. Patel, W. I. White, J. F. Young, and P. A. Kiener.** 2007. Development of motavizumab, an ultra-potent antibody for the prevention of respiratory syncytial virus infection in the upper and lower respiratory tract. J. Mol. Biol. **368:**652–665.
44. **Wu, S.-J., A. Schmidt, E. J. Beil, N. D. Day, P. J. Branigan, C. Liu, L. L. Gutshall, C. Palomo, J. Furze, G. Taylor, J. A. Melero, P. Tsui, A. M. Del Vecchio, and M. Kruszynski.** 2007. Characterization of the epitope for anti-human respiratory syncytial virus F protein monoclonal antibody 101F using synthetic peptides and genetic approaches. J. Gen. Virol. **88:**2719–2723.
45. **Yin, H.-S., R. G. Paterson, X. Wen, R. A. Lamb, and T. S. Jardetzky.** 2005. Structure of the uncleaved ectodomain of the paramyxovirus (hPIV3) fusion protein. Proc. Natl. Acad. Sci. U. S. A. **102:**9288–9293.
46. **Yin, H. S., X. Wen, R. G. Paterson, R. A. Lamb, and T. S. Jardetzky.** 2006. Structure of the parainfluenza virus 5 F protein in its metastable, prefusion conformation. Nature **439:**38–44.